Order parameters in the diffusion of rods through two- and three-dimensional fixed scatterers

Benjamin D. Mahala and Rigoberto Hernandez

Order parameters in the diffusion of rods through two and three dimensional fixed scatterers

Benjamin D. Mahala[1] and Rigoberto Hernandez[1, *]

[1]*Department of Chemistry, The Johns Hopkins University, Baltimore, MD*

(Dated: September 28, 2018)

Abstract

Characteristic diffusion in a Lorentz Gas system and its extensions are typically described through a scale-free order parameter. The relative validity of possible order parameters for the diffusion of a thick tracer rod through spherical scatterers in two and three dimensions as a function of the rod length L and scatterer density ρ has been examined by simulation. We find that the often-used two-dimensional order parameter, ρL^2, is accurate. However, its naive generalization to three dimensions, changing the exponent according to dimensionality, does not fit the observed results. A revised order parameter can be generated through a theory based on the behavior of the mean free path of the tracer. We find that this generalized order parameter captures the multidimensional diffusive behavior.

---

* E-mail: r.hernandez@jhu.edu

I. INTRODUCTION

Characterization of the diffusion of prolate particles through a solvent is layered in complexity. The asymmetry of the particle structure can lead to asymmetry in its diffusion if the solvent is not uniformly distributed at some characteristic length scale shorter than that of the particle. The nontrivial rotations of the particle about its secondary axes contributes to the dynamics in ways that could lead to asymmetric transport. The nature of the complex solvent can also significantly affect the dynamics of the particle. For example, it could be structured or dissipative in ways that alter its relative rotation, libration, motion along the primary axis direction, and motion across the secondary axes directions. Unraveling this problem does not simply address an interesting theoretical model because, for example, small cylindrical particles are common nanomaterials that have unique electronic properties that are affected by their relative structure and assembly. They often exhibit interesting surface plasmon resonances that can be used for a variety of applications, including lasers and catalysts.[1, 2]

We, and others, have used the Lorentz gas (LG) model to describe the solvent as a set of fixed scatterers.[3–8] The LG model was originally introduced by Lorentz in 1905 to model the transport of electrons in a metal and from which he derived a linear Boltzmann equation.[9] The model was used to elaborate the diffusion of light fast particles —the wind— across heavy immovable particles —the trees— so to rigorously construct correlation functions for the corresponding kinetic gas systems.[10] Since then, the LG model has served as a useful benchmark system for kinetic and dynamical theories.[11] The model is simple enough that it is often analytically tractable, if not exactly solvable, and simulations of it are computationally inexpensive. In the context of this work, the LG model describes the environment for the motion of a prolate cylindrical particle through a sea of heavy immobile scatterers organized in either a periodic or aperiodic fashion. The dynamics of the tracer particle in the LG system exhibits surprisingly complex transport behavior. It was discovered early on that the transport coefficients for the LG model system are non-analytic functions of the density, and that any density expansion would diverge in the Dth term where D is the system dimensionality.[12]

For equilibrium structural properties, this model system scales according to a single order parameter, $n^* = \rho\sigma^D$, where σ is the radius of the scatterers and ρ is the density.[12–15]

Extensions addressing rods with more complex geometries and self-propulsion have also been explored and is of current interest because of recent advances in the characterization of active matter.[7, 16–20] The spherical-tracer order parameter is typically extended for a rod in spheres to 2 and 3 dimensions as $n^* = \rho L^D$ where L is the length of the tracer rod.[21] In this article, we aim to characterize the dynamics of such structured particles within the LG model and test the hypothesis that this or a new modified order parameter provides the appropriate scaled dynamics.

In earlier work by Tucker and Hernandez,[7] the possibility of excluded volume effects on the dynamics of the diffusing particle was introduced into the model by extending the representation of the particle or scatterers from points to spheres, preserving the spherical symmetry of the point particle, but giving it a width. The possibility of effects due to nonspherical structure in the scatter can be introduced by allowing the particle to be a rod with zero radius. One might expect translational diffusion to be a monotonically decreasing function of the density. However, when the motion of a rod-like particle was investigated by Franosch and coworkers[6, 22] an enhanced diffusion regime was discovered in a rod moving through an LG model with point particle scatterers. In this enhanced diffusion regime, increasing the scatterer density leads to increased translational diffusion.[6] An enhanced diffusion regime was also seen for a dense solution of infinitely thin rods due to confinement,[23] though absent in the case of thick scatterers.[8]

Moreno and Kob[3, 4] addressed a thick rod LG model with thick (and non-overlapping) spheres that led to glassy dynamics with increasing density. Tucker and Hernandez[7] addressed a thick rod with point scatterers in two dimensions; finding that both enhanced diffusion and glassy regimes were accessible. In attempting to generalize to higher dimensions, however, we found that the order parameter n^* is no longer satisfactory.

In Sec. II, we summarize the LG model for a rod diffusing through spheres, the structure of its transport coefficients, and the order parameters that have been used to characterize it. The framework and parameters of our simulations are presented in Sec. III. We report the simulation data in Sec. IV, and introduce a correction to the order parameter to correct for the differences in the mean free path that we found in three dimensions rather than two. This, in turn, leads to a hypothesis for a useful order parameter in three dimensions which is a central result of this article.

II. THEORY

A. The LG Model

The LG model in this work consists of a mobile tracer and a sea of immovable scatterers. The tracer moves ballistically between scatterers until it comes into contact with a scatterer and experiences a hard collision. Over time, the tracer experiences diffusive motion through the scatterer background, giving rise to a well-defined diffusion constant.

The tracer is described by a cylinder of length L and radius σ_t with end caps made of hemispheres of the same radius σ_t. It has a total mass M and uniform density. The scatterers are a sea of immobile spherical particles with radius σ_s. They are placed randomly in the box at homogeneous density ρ, and are allowed to overlap. The tracer dynamics is either that of ballistic motion between collisions or hard elastic collision upon contact with a scatterer. In the simulations, a finite size D-dimensional box with sides of length L_{box} satisfying periodic boundary conditions is used to represent the infinite extent of the formal system. Simulations with varying L_{box} confirmed that there were no finite size effects. The tracer is placed in a random position and orientation within the periodic box. If that selection overlaps with a scatterer, the tracer is removed and placed randomly again. After 10,000 attempts to find a non-overlapped position, the scatterer background was re-created, and the iteration to place the tracer was re-initiated. Such reboots of the scatterer positions were rarely needed to find an initial tracer position even at the largest scatterer densities considered here.

The tracer is given a random translational and rotational velocity taken from independent Maxwellian distributions with temperature T. It can then be propagated by the classical equation of motion with the only interactions arising from the hard collisions—either head-on or glancing—between the rod and the scatterers.

B. Transport Coefficients

The transport coefficients for tracers diffusing across a random LG model can be derived analytically in certain limiting cases. For a random scatterer background, the analytic form of the diffusion constant has been computed in 2D for the low density case.[3] Specifically, Moreno and Kob[3] obtained the low-density diffusion limit from kinetic theory and mode coupling theory for a 2D medium with point obstacles following approach similar to Ref. 14.

They also added a correction factor for moderate densities, resulting in the reduced diffusion constant,

$$D_{\mathrm{com}}/D^0_{\mathrm{com}} = 1 + (32/9\pi)\rho^*\ln\rho^* \tag{1}$$

where

$$D_{\mathrm{com}} = \frac{3\langle v \rangle}{16\rho R} \tag{2}$$

$$p^* = \rho R^2 \tag{3}$$

$$R = (L_{\mathrm{Kob}} + (\pi - 1)\sigma)/\pi \tag{4}$$

In their model, the rigid rod was represented by N point-wise beads of mass m placed in a straight line with intervals spacings of 2σ. The length of the rigid rod is consequently described by $L_{\mathrm{Kob}} \equiv 2(N-1)\sigma$. They set the size of their scatterers to zero without loss of generality by way of renormalizing the effective length of the rod as $R = (L_{\mathrm{Kob}} + (\pi - 1)\sigma)/\pi$.

The model of Moreno and Kob can be mapped to the thick rod and LG scatterers discussed here through the following set of transformations:

$$L = L_{\mathrm{Kob}} + \pi\sigma \tag{5}$$

$$n^* = \frac{\rho(L_{\mathrm{Kob}} + \pi\sigma)}{\pi^2} , \tag{6}$$

where L and σ are the length and radius of the thick rod. Note that, unlike in our LG systems, their scatterers are not allowed to overlap. Our 2D results are compared to these theoretical values in Sec. IV, and the agreement is generally good at lower densities. The theory fails to have agreement at higher scatterer densities where both the differing nature of the scatterers and the excluded volume of the particle play an important role.

C. Order Parameters

In general, the reduced diffusion constant scales as

$$D_{\mathrm{red}} \propto v\lambda \tag{7}$$

where v is the average velocity of the center of mass of the rod and λ is its mean free path obtained for sufficiently long trajectories. The mean free path is inversely proportional to

the product of the density of scatterers and the tracer-scatterer collision cross-section. For a 2D needle with length L moving though a sea of point scatterers, the mean free path is proportional to $\frac{1}{\rho L}$, where ρ is the density of scatterers. The cross-section is the length of the tracer. Insertion of the mean free path into Eq. 7 and division by vL results in a reduced diffusion constant which scales as

$$D_{\text{red}} \propto \frac{1}{\rho L^2} \tag{8}$$

$$\propto \frac{1}{n^*} \tag{9}$$

This suggests that n^* is a good order parameter for the system in 2D.

In three dimensions, the situation is different. The mean free path of a needle with length L and thickness σ though a sea of point scatterers is given by $\frac{1}{\rho L \sigma}$ because the cross-section is proportional to the areas of the rectangle $L\sigma$. Applying the same transformations as before to obtain the reduced diffusion constant gives:

$$D_{\text{red}} \propto \frac{1}{\rho L^2 \sigma} \tag{10}$$

$$\propto \frac{1}{\frac{\sigma}{L} n^*} \tag{11}$$

This implies that $\frac{\sigma}{L} n^*$ would make a good order parameter for 3D. We take the ratio $\frac{\sigma}{L}$ to be a correction factor γ on the reduced diffusion n^* to create a new order parameter: γn^*. We show in Sec. IV that this new order parameter provides the desired invariance in our test simulations.

III. NUMERICAL METHODS

A. Numerical Integration and Propagation

The integration algorithm for the evolution of the tracer under the classical equation of motions is simplified by the fact that the motion is ballistic as long as there is no collision. The algorithm used here is time-step based, evolving the system forward in time in successive steps at constant velocity and correcting those steps which involved a scatterer-tracer collision through a careful accounting of the collision event.[7, 8] Even at the highest densities explored in this work, the frequency of these collisions, relative to our time step, were sufficiently low that the calculations could be performed in reasonable time.
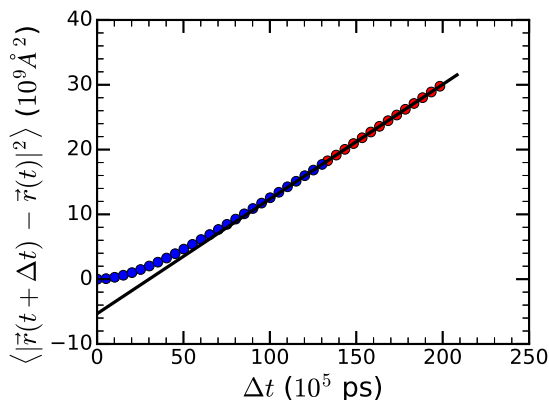
FIG. 1. A typical MSD (blue and red dots) for a 2D simulation as a function of displacement time Δt. Specifically, the parameters are: $n^* = 0.1$, $L = 14.142$ Å, $\sigma_s = 0.5$Å, $\sigma_t = 0.5$Å. The blue points are those excluded from the fitting due to not being in the linear regime. The black line is the linear fit of the red points with a slope of 1769.02 ± 0.24 ps.

Although an event-driven molecular dynamics integrator can be more efficient then a time step based integrator [24], we want to be able to sample data at shorter time scales then the collision time scale; and, as such need discrete time steps independent from the collision rate. Once a collision has been detected, the tracer's motion is reversed until it has reached the point of contact, where the equations for a hard collision are applied. After a set amount of time the position and velocity of the tracer is recorded for data collection and analysis. After a set number of time steps, which corresponds to a given amount of real time, another scatterer background is generated, the tracer's position and velocity is regenerated, and a new trajectory is started. After all of the trajectories are complete, the relevant correlation functions are calculated and the transport coefficients are extracted. The numerical integration of trajectories and averaging of the correlation functions are done with in-house Fortran code; the fitting and plotting with in-house Python code.

Each of the trajectories reported here were integrated on the first-generation XSEDE Stampede CPU nodes (2.7 GHz Xeon E5-2680 8-core Sandy Bridge processors with the Intel Xeon Phi SE10P KNC MIC coprocessor), and completed on one core in less then 24 hours of processing and analysis time.
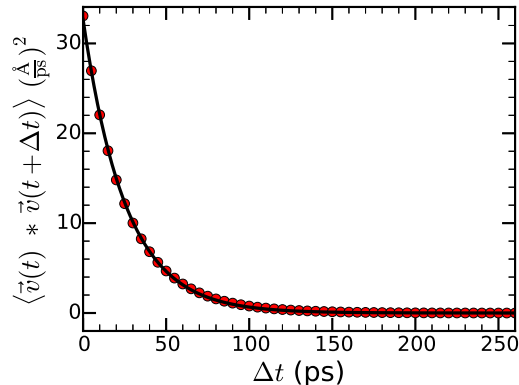
FIG. 2. A typical velocity autocorrelation function (red dots) for a 2D simulation as a function of displacement time Δt at the same parameters as in Fig. 1 The black line is the exponential fit with a decay time of 25.615 ± 0.009 ps.

B. Algorithms for Determining Transport Coefficients

The translational diffusion constant D_{com} is extracted via three different methods: (i) using a linear fit of the long time mean square displacement (MSD) as illustrated in Fig. 1 for a particular set of parameters, (ii) using a two variable power law fit of the long time MSD, and (iii) through integration of the velocity autocorrelation function.

In the first and second method, we take advantage of the relationship between the diffusion constant and the MSD given by the Brown-Einstein-Smolouchowski relation,

$$D_{\text{com}} = \frac{1}{2D} \lim_{\Delta t \to \infty} \frac{d}{d(\Delta t)} \langle (\vec{r}(t + \Delta t) - \vec{r}(t))^2 \rangle_t \tag{12}$$

where D is the dimensionality of the system. Note that $\langle ... \rangle_t$ is an average over all time t. The use of Δt for several prior t's instead of the fixed starting point at $t = 0$ allows for enhanced averaging.

D_{com} can then be extracted numerically from the mean-square displacement. In the first method, we fit the long time MSD to a line whose slope is $2DD_{\text{com}}$. In the second method, we account for the possibility that the finite size of the data can cause convergence errors leading to apparent anomalous diffusion. The corresponding assumption of a power law form —with m and α as the prefactor and exponent, respectively— for the position correlation

8

function in Eq. 12 leads to an intermediate time approximation of the diffusion constant,

$$D_{\text{com}} = \frac{1}{2D} \frac{d}{d\Delta t} (m\,\Delta t^{\alpha}) \bigg|_{\Delta t \approx t^*} \tag{13}$$

where t^* is a characteristic time associated with the intermediate region where the power law is fit to the data, and we approximate it as the median of the times in the fitting window. After simple algebra, we find that the diffusion constant is

$$D_{\text{com}} \approx D_{\alpha} (t^*)^{\alpha-1} \tag{14}$$

where $D_{\alpha} \equiv \frac{\alpha m}{2D}$. For a Brownian (or any nonanomalous) system, as $t^* \to \infty$ then $\alpha \to 1$. Consequently, Eq. 14 reduces to $D_{\text{com}} = D_{\alpha}$, which is the expected limiting behavior.

A typical fit of the velocity autocorrelation data is shown in Fig. 2. The relationship between the velocity autocorrelation function (VAC) and D_{com} is given by the following Green-Kubo relation:

$$D_{\text{com}} = \frac{1}{D} \int_0^{\infty} \langle \vec{v}(t+\Delta t)\vec{v}(t)\rangle_t d(\Delta t) \tag{15}$$

where D is the dimensionality of the system. The use of the integrand as an average over t for each given Δt is not formally necessary, but it is numerically useful as it allows for more points to contribute to the numerical integral.

C.   Numerics in Determination of Diffusion Coefficients

The diffusion constant can be obtained from numerically determined MSDs such as that shown in Fig. 1. At intermediate times —beyond the initial inertial regime and before the end of the trajectories,— the system exhibits diffusive behavior and satisfies a form linear in time. $\left\langle (\vec{r}(t+\Delta t) - \vec{r}(t))^2 \right\rangle \approx v_0 \Delta t$. Insertion into Eq. 12 yields the diffusion constant,

$$D_{\text{com}} = \frac{v_0}{2D} \tag{16}$$

For example, the slope v_0 of the MSD in Fig. 1 is 1769.0 ± 0.2 Å/ps. Consequently, the diffusion rate obtained from the linear MSD plot is $442.25 \pm 0.06\ \frac{\mathring{A}^2}{ps}$.

Alternatively, the fits can be performed on a log-log representation of the data. From the data shown in Fig. 1, such a log-log fit led to the optimized parameters: $t^* = 1.67\ \mu s$, $\alpha = 1.230 \pm 0.006$, and $D_{\alpha} = 16.6\ \frac{\mathring{A}^2}{ps}\frac{1}{ps^{\alpha}}$. Use of Eq. 14 yields the diffusion constant, $D_{\text{com}} = 444.66 \pm 39.0\ \frac{\mathring{A}^2}{ps}$. Note that these error bars are much larger than the error for the linear

fit, since the linear fit assumes the exponent α is exactly 1, so error in the determination of this exponent is not propagated.

Alternatively, the diffusion constant can be obtained from the VAC function. We approximate it as a single exponential $\langle v^2 \rangle e^{-t/\tau}$ where τ is the decay time. The diffusion constant of Eq. 15 then reduces to:

$$D_{\text{com}} = \frac{\langle v^2 \rangle}{Dv_0} = \frac{2kT\tau}{Dm} \tag{17}$$

The values of the fitting parameters for the same case as in Fig. 1 are: $\langle v^2 \rangle = 32.680 \pm 0.008$, and $\tau = 25.615 \pm 0.009$ with the effective dimensionality of the system set to 2. As such, one recovers a diffusion constant equal to $418.54 \pm 0.04 \, \frac{\mathring{A}^2}{ps}$.

The values of the diffusion constants obtained from the linear MSD and VAC fits are much larger than the width of the error bars. However, the diffusion constant obtained from the VAC is on the order of the error seen in the log MSD fit. This is due to the linear MSD and VAC error calculations not accounting for convergence error. We take the variance for all of our averages when computing the MSDs and VAC. We then use these variances to judge the error in the fit for the MSD and VAC fitting. This method works well for estimating noise in the fitting itself. However, to compute the diffusion exactly, we would need to take averages at infinitely long time with infinitely fast velocity sampling. Since our samples are of finite size, there is convergence error in the diffusion constant that is not represented in the variance of the individual data points in the linear MSD and VAC. An illustration of the convergence with increasing number of scatterers is shown in Fig. 3 for two representative cases in 2D and 3D. We thus extract the diffusion constant via the three approaches in order to obtain an estimate of the relative accuracy of the numbers in a way that would not be represented by the apparent convergence of a given approach, and report the numbers accordingly.

IV. RESULTS

A. Tracer in Two Dimensions

The reduced diffusion constant at constant n^* for three different n^* and three different cases of the characteristic lengths L_0 of the diffusing rod is shown in Fig.4. The values L_0, noted in the figure caption, are characteristic in the sense that they represent the regime
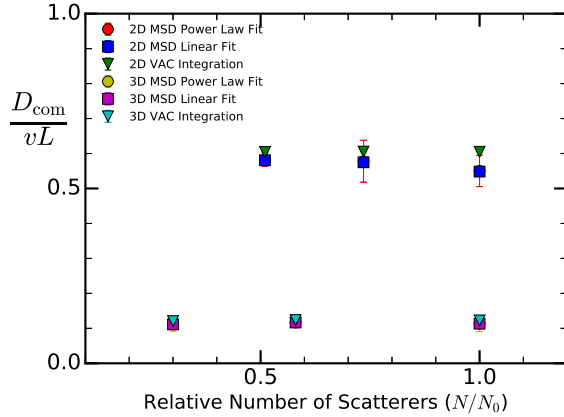
FIG. 3. The 2D and 3D diffusion constants obtained on a periodic box with increasing size and corresponding increasing number of scatterers. The tracer length is held fixed at $L = 31.623$Åand 21.544 Åin 2D and 3D, respectively. The number of scatterers in the largest finite box is N_0 equal to 1960 and 3375 in 2D and 3D, respectively. In all cases, the box size and N satisfy the condition that the scatterer density is 0.001, and $n^* = 1.0$.

(at sufficiently large lengths) when the diffusion constant has plateaued for each given n^*. The observed reduced diffusion at constant n^* exhibits similar behavior over a wide range of densities, including in the enhanced diffusion regime. In particular, they exhibit a horizontal asymptote for values with a constant diffusion constant at large tracer length. This is consistent with the hypothesis that n^* is a good order parameter for the system in this regime, since the reduced diffusion is a function of n^* alone.

However, n^* is not a good order parameter at low L as indicated by the depression in the curve towards zero at zero L. At constant n^*, a decrease in L implies an increase in number density, but a decrease in collision cross section such that the overall reduced diffusion in unchanged. For a system with space filling rods and scatterers, L is not the only variable that determines the cross section. At zero L, the tracer is a sphere of radius σ_t, surrounded by spheres of radius σ_s. In this limit, the diffusion goes to zero. To fix this, σ_t and σ_s must change to hold the cross section constant as L decreases. We create a new effective L such that:

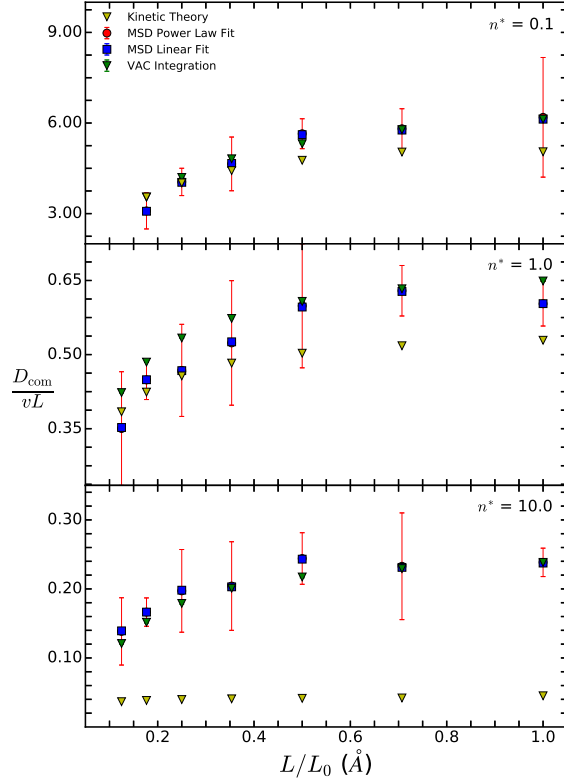$$L_{\text{eff}} = L + 2\sigma_s + 2\sigma_t \tag{18}$$

11

FIG. 4. The 2D reduced diffusion constant as a function of tracer length at three different constant values of n^* scaled by a characteristic length $L_0 = 28.3$, 63.2 and 200 in each panel from top to bottom, respectively. Notice that the reduced diffusion is a good order parameter at large tracer length (low density at constant n^*) because the curves are flat in this region, and hence D_{com} is a constant with respect to L.

and from this create an effective n^*:

$$n^*_{\text{eff}} = \rho L^D_{\text{eff}} \tag{19}$$

As shown in Fig. 5, This n^*_{eff} is a good order parameter in 2D, as it correctly accounts for the cross section of the tracer when it is not dominated by L alone.
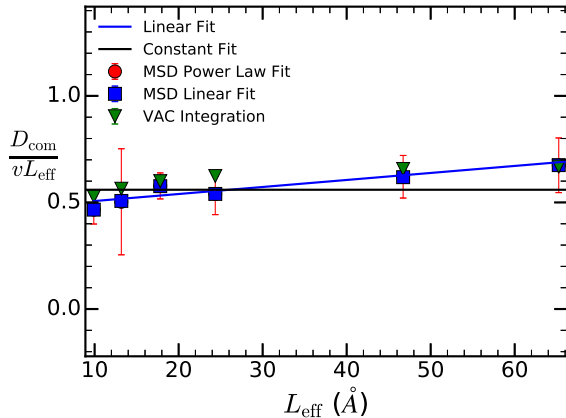
12

FIG. 5. The dependence of the 2D translational diffusion constant of the tracer on the effective length L_{eff} at constant n^*_{eff}. In this case $n^*_{\text{eff}} = 1.0$, $\sigma_s = \sigma_t = 0.5$. The blue line is the linear fit, and the black line is a constant fit. The constant fit is within the error bars of the power law fit, $\frac{D_{\text{com}}}{vL_{\text{eff}}} \sim .003 \ L_{\text{eff}}$, which is within 1.5 σ from zero.

B. Tracer in Three Dimensions

The reduced diffusion constant in 3D for three values of n^* is plotted in Fig. 6. The L_0 values refer to the largest lengths of the tracer considered here for three-dimensional scatterers at a particular n^*. Their values were chosen to correspond to the two dimensional cases of the previous subsection. The most obvious difference to the trends seen in 2D is that there is only one regime, and it is linear. This implies that in three dimensions, n^* is not a good order parameter in any limit because it cannot uniquely predict the diffusion constant. Correcting for excluded volume does not help the situation either. When the excluded volume is accounted for, the diffusion is still a strong function of the scatterer length at constant n^*_{eff}, as shown in Fig. 7.

A simple fix would be to attempt to find a length scale that is proportional to L. However, this would not lead to a flat curve. The linearity could only be reduced to a constant via division by L if the y-intercept of the linear fit were zero. This is not the case for any of the n^* observed.
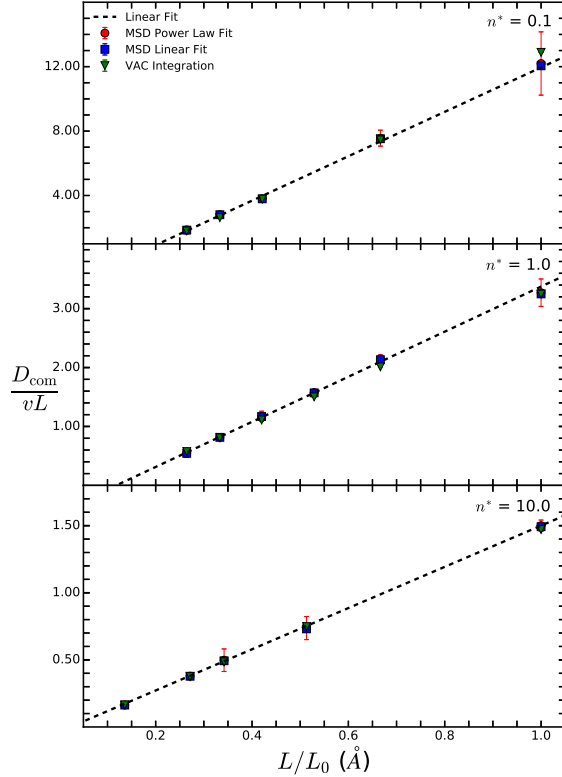
FIG. 6. The 3D reduced diffusion constant as a function of tracer length at constant values of n^* —as also displayed for the 2D case in Fig. 4— scaled by a characteristic length $L_0 = 7.0$, 29.2, 63.0 from top to bottom, respectively. The dashed line is a linear fit to the data, with R^2 values > 0.999 for all plots. Note that the reduced diffusion is nowhere a good order parameter in 3D.

V. DISCUSSION

A new order parameter γn^* for the diffusion of rods through scatterers in three dimensions was constructed in Sec. II. The need for this scaling law lies in its use to surmise and predict the behavior of these systems with a minimum number of characteristic degrees of freedom in the parameter space. These considerations, and their relevance to experiment, are our primary motivation for its construction and elaboration.

To numerically confirm that γn^* is indeed a good order parameter, the diffusion constant was determined or various values of L, σ, and ρ and summarized in Fig. 8. A surface was
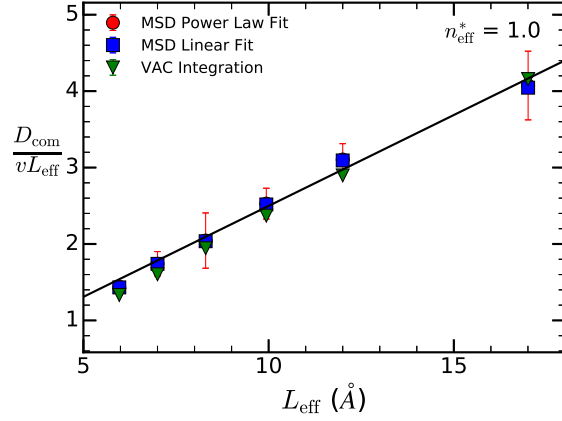
14

FIG. 7. The 3D translational diffusion constant of the tracer as a function of the effective tracer length L_{eff} at constant n^*_{eff}. The parameters are $n^*_{\text{eff}} = 1.0$, $\sigma_s = \sigma_t = 0.5$. The black line is the linear fit, $\frac{D_{\text{com}}}{vL_{\text{eff}}} \sim .24 \ L_{\text{eff}}$, with a slope that is about 100 times that in the 2D case.
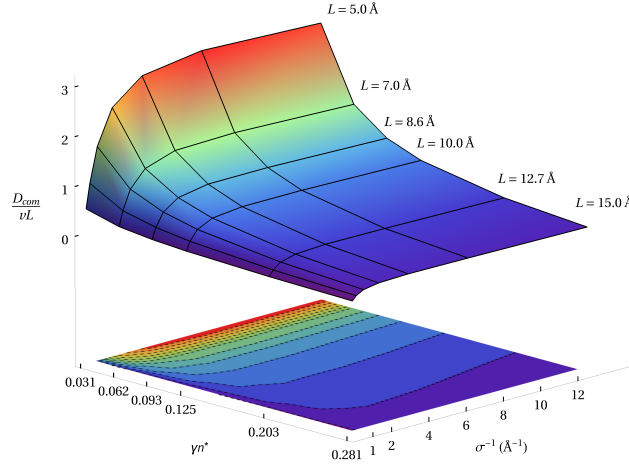

FIG. 8. The 3D reduced diffusion constant is displayed as contour and 3D-surface plots over the two-dimensional domain of γn^* and scatterer and tracer radius σ^{-1}. The black lines on the surface indicate constant L as indicated, and also correspond to the values of γn^* on the bottom left axis. The vertices of the lines on the upper surface are explicitly computed to which the surface has been fitted. The dashed contour lines represent lines of constant reduced diffusion and potential order parameters.

15

extrapolated over the set of resultant reduced diffusion points. The surface is indeed nearly constant over domains with constant values of γn^* suggesting that this quantity is a good order parameter across most of these three-dimensional systems.

These models are applicable to the classical diffusion of rod-like molecules on surfaces. For example, Fichthorn and coworkers found that the dynamics of dimers on medal surfaces can be complex and highly dependent on the relative shape and size of the dimer and geometry of the underlying surface. [25–27] While the present work does not explicitly consider inhomogeneities due to an an underlying surface in the 2D case, it does consider the inhomogeneities in the plane of the surface are represented by the scatterers. Perhaps not surprisingly, we found similar complexity, but have added the possibility of corresponding behavior as captured though the scaling law.

The diffusion of a rod in an environment with controlled scatterer density is experimentally realizable, and its existence has motivated, in part, much of the work by other groups and us. For instance, Roichman et al[28] follow the dynamics of a single silver nanowire confined to two dimensions as it diffuses through a set of randomly generated repelling focused laser beams or polymer pillars. Their rods experience viscous and hydrodynamic effects that are not included in the simple models of this work. Indeed, these effects lead to a breakdown of the scaling laws that we have found here, thereby illustrating the need for including such effects. Similarly, Composto and coworkers[29] observed the diffusion of a titanium dioxide nanorod though a polystyrene melt where the length and thickness of the nanorod is comparable to the radius of gyration of the polymer melt. They found that the translational diffusion of the nanorod can be up to three orders of magnitude faster than what would be expected from a uniformly distributed environment in which the rod diameter is smaller than the entanglement mesh size. Recognizing that their nanorods are constrained by the polymer in a similar way to how our rods are constrained by scatterers, this is evidence for the enhanced diffusion our group[7] observed earlier. Moreover the 3 dimensional nature of the confinement of the polymer network allows for enhanced diffusion to persist even in three dimensions when a disconnected network of scatterers does not lead to it.[8] Once again, this analysis is clearer because of the differences observed in systems with putative corresponding order parameters that break down because of the additional complexities of the actually system. Thus, the current findings afford us a new way to better characterize the nonadditive effects that emerge from increased complexity in the diffusing

medium or the scatterer network.

Finally, the scatterers in this work were arranged in the periodic box using a homogeneous random selection that permits naive overlaps. One possible concern is how a different selection of the scatterers would affect the results and the associated scaling law. The placement of the scatterers clearly presents the possibility for different dynamics. For example, if the scatterers were so heterogeneously placed so as to leave large and simply connected regions free of scatterers, the rod would diffuse ballistically within said regions deterred only slightly by a search through the interconnections, and thus diffuse faster. The scaling behavior found here may still be relevant in selected regimes, but proving this would require additional effort beyond the scope of this work.

VI. CONCLUSIONS

In this article, we have determined how the reduced diffusion constants for a particle moving through an isotropic random LG scatterers differ between two and three dimensions. We have summarized the features necessary for identifying good order parameters as previously used to describe related systems, and obtained the corresponding order parameters for a spherocylinder solvated in a Lorentz gas of spherical particles. In two dimensions, the reduced density makes a good order parameter so long as excluded volume is properly accounted for. However, in three dimensions, the naive extension of the two-dimensional order parameter is insufficient to characterize the system. An approach accounting for excluded volume effects does not lead to an appropriate order parameter with invariant properties. We found that this is due to the failure of the two-dimensional order parameter to include the effects of the changes in the mean free path of the tracer in three dimensions. We derived and benchmarked the corrected 3D order parameter by extending the 2D order parameter using the correct scaling behavior of the mean free path with dimensionality.

The existence of an appropriate order parameter for these systems in two and three dimensions does more than provide a reduced variable with which to characterize them. It also suggests a mechanism by which the cylindrical tracer generally diffuses through the scatterers. In two dimensions, the motion of the rod tangentially to its parallel axis is confined by its length L whereas in 3 dimensions a small perturbation above or below the scatterer allows it to go freely past a would-be scatterer. Such different physics results in the

17

rather different order parameters that we have observed here for two- and three-dimensions.

VII.   ACKNOWLEDGMENTS

[1] A. L. Schmucker, N. Harris, M. J. Banholzer, M. G. Blaber, K. D. Osberg, G. C. Schatz, and C. A. Mirkin, ACS Nano **4**, 5453 (2011).

[2] B. S. Hoener, C. P. Byers, T. S. Heiderscheit, A. S. D. S. Indrasekara, A. Hoggard, W.-S. Chang, S. Link, and C. F. Landes, J. Phys. Chem. C **120**, 20604 (2016).

[3] A. J. Moreno and W. Kob, Europhys. Lett. **67**, 820 (2004).

[4] A. J. Moreno and W. Kob, J. Chem. Phys. **121**, 380 (2004).

[5] F. Höfling and T. Franosch, Phys. Rev. Lett. **98**, 140601 (2007).

[6] F. Höfling, E. Frey, and T. Franosch, Phys. Rev. Lett. **101**, 120605 (2008).

[7] A. K. Tucker and R. Hernandez, J. Phys. Chem. B **114**, 9628 (2010).

[8] A. K. Tucker and R. Hernandez, J. Phys. Chem. B **115**, 4412 (2011).

[9] H. A. Lorentz, Proc. Amst. Acad. **7**, 438 (1905).

[10] G. Gallavotti, Phys. Rev. **185**, 308 (1969).

[11] C. P. Dettmann, Commun. Theor. Phys. **62**, 521 (2014).

[12] J. M. J. Van Leeuwen and A. Weijland, Physica **36**, 457 (1967).

[13] R. Zwanzig, Phys. Rev. **129**, 486 (1963).

[14] W. Götze, E. Leutheusser, and S. Yip, Phys. Rev. A **24**, 1008 (1981).

[15] C. Bruin, Physica **72**, 261 (1974).

[16] A. K. Tucker and R. Hernandez, J. Phys. Chem. B **116**, 1328 (2012).

[17] H. Khalilian and H. Fazli, J. Chem. Phys. **145**, 164909 (2016).

[18] M. Zeitz, K. Wolff, and H. Stark, Eur. Phys. J. **40**, 23 (2017).

[19] S. A. Mallory, C. Valeriani, and A. Cacciuto, Phys. Rev. E **90**, 032309 (2014).

[20] C. Tung, J. Harder, C. Valeriani, and A. Cacciuto, Soft Matter **12**, 555 (2016).

[21] D. Frenkel and J. F. Maguire, Phys. Rev. Lett. **47**, 1025 (1981).

[22] T. Munk, F. Höfling, and T. Franosch, Europhys. Lett. **85**, 30003 (2009).

[23] S. Leitmann, F. Höfling, and T. Franosch, Phys. Rev. E **96**, 012118 (2017).

[24] M. N. Bannerman, R. Sargant, and L. Lue, J. Comput. Chem. **32**, 3329 (2011).

[25] R. Wang and K. A. Fichthorn, Phys. Rev. B **48**, 18288 (1993).

[26] J.-C. Wang and K. A. Fichthorn, Langmuir **12**, 139 (1996).

[27] A. Ramirez-Pastor, M. Nazzarro, J. Riccardo, and V. Pereyra, Surf. Sci. **391**, 267 (1997).

[28] Y. Roichman, A. Waldron, E. Gardel, and D. G. Grier, Appl. Opt. **45**, 3425 (2006).

[29] J. Choi, M. Cargnello, C. B. Murray, N. Clarke, K. I. Winey, and R. J. Composto, ACS Macro Lett. **4 (9)**, 952 (2015).